Research article

Characterizing unusual metal substrates for gap-mode tip-enhanced Raman spectroscopy

Johannes Stadler,[a] Benedikt Oswald,[b] Thomas Schmid[a] and Renato Zenobi[a]*

In this article, the electromagnetic (EM) field in gap-mode tip-enhanced Raman spectroscopy (TERS) is investigated theoretically and experimentally for a range of commonly used and unusual metal and nonmetal substrates. By approaching a metal tip to a substrate, both form a coupled system that confines the EM field created at the tip apex. The influence of the substrate onto the EM field enhancement is observed in a top-illumination gap-mode TERS setup for different metal substrates. These include Au, the most commonly used substrate, and also a wide range of rarely or previously unused TERS substrates (Cu, Ag, Al, Pd, Pt, Ni, Ti, Mo, W, stainless steel, Al_2O_3, SiO_2). Self-assembled monolayers of thiols and brilliant cresyl blue thin film samples are investigated experimentally on nine metal substrates, all showing considerable TERS enhancement. With finite difference time domain and finite element simulations used, the article provides a good estimate of the EM field enhancement for a wide range of substrates for users to estimate how well a substrate of choice will perform in a gap-mode TERS experiment. The reduction in EM field strength $|E^2|$ compared with Au is less than an order of magnitude for many metals (Calculations: Cu 92%, Ag 81%, Ni 53%). This article experimentally shows that a wide variety of conductive substrates can be used, when one is willing to trade a fraction of the EM field enhancement. TERS was seen on all metal substrates including stainless steel, yet quantification was not always possible. These qualitative results were complemented with intensities from calculations. The wider variety of substrates will increase the applicability of TERS and evolve it one step further towards use in standard analytics. Copyright © 2012 John Wiley & Sons, Ltd.

Supporting information may be found in the online version of this article.

Keywords: tip-enhanced Raman spectroscopy; plasmonics; simulations; finite elements; finite difference time domain

Introduction

Tip-enhanced Raman spectroscopy (TERS) is a powerful emerging analytical tool for chemical analysis on the nanometer scale. TERS was first described in 2000 in several publications that employed different geometries.[1–4] TERS on the one hand benefits from the large information content of a spectroscopic technique; that is, it allows identification of molecules from their vibrational fingerprint spectrum. Yet, in contrast to conventional Raman spectroscopy, it surpasses the two major drawbacks of Raman, that is, the bad sensitivity due to the intrinsically small cross section of the Raman process and the limited resolution due to diffraction of light. This is achieved by introducing a metal or metal-coated sharp tip into the illumination laser focus and approach it to within a few nanometer of the sample. Several distance control methods can be used to control the position of the tip. In this approach, we employ scanning tunneling microscopy (STM) for which a conductive substrate is a prerequisite. Upon illumination of the TERS tip with a focused laser beam, a dipole is induced in the tip apex. Because of the proximity of the tip to the metal substrate, mirror charges are accumulated at the surface of the metal substrate that can be described by an image dipole. The strong, very localized electromagnetic (EM) field in the gap between the tip and substrate is used as a nanometer-sized light source for the experiments, hence the name gap-mode STM-TERS. In almost all published gap-mode STM-TERS results, Au has been used as a substrate. It combines several advantages, for example, chemical inertia, sufficient substrate flatness[5] as well as a low imaginary part of the dielectric constant ε_2 (attributed to losses) in the visible optical region. With Au surfaces used, an efficient enhancement can be reached in conjunction with etched full

metal tips from Ag[6–8] or Au wires.[9–11] Yet, the production of very flat and pure Au substrates is cumbersome and expensive. Limitation to gold substrates is a drawback because of incompatibility with certain samples and also negates the possibility to investigate samples directly during production on their native substrates. In this article, the impact of the substrate metal on the TERS process should be investigated experimentally as well as theoretically. Previous calculations mostly investigated the influence of the dielectric constant of the tip,[12] the shape,[13] or the influence of the tip-sample distance[14–16] on the EM field in the gap between the tip and the sample. Calculations on the intensity of the EM field as a function of the dielectric constant (Drude model[17,18]) have been presented by Zhang et al.[19] using a simplified single oscillator dipole model. For three different substrates, Au, Pt and SiO_2, coarse field simulations with tip were presented by Yang et al.[16]

Experimentally, Au is used in most experiments as sample support for STM-TERS experiments. It has been used in side-illumination and top-illumination experiments, with both objective lenses and a parabolic mirror as focusing element.[20–25] Only a few isolated examples can be found in the literature on TERS with STM distance control where substrates other than Au have been

* Correspondence to: Renato Zenobi, ETH Zurich, Department of Chemistry and Applied Biosciences, Wolfgang-Pauli-Strasse 10, HCI E-329, 8093 Zurich, Switzerland. E-mail: zenobi@org.chem.ethz.ch

a ETH Zurich Department of Chemistry and Applied Biosciences, Wolfgang-Pauli-Strasse 10, HCI E-329, 8093 Zurich, Switzerland

b Paul-Scherrer Institut, WBGB 131, 5232 Villigen, Switzerland

employed: Ag,[26] Ni,[27] Pt,[28] and Cu[29] have been successfully used in TERS experiments. The reasons to use metals other than Au were usually sample specific. In the case of Ag, special binding properties were used to attach the sample; with Cu, the metal is part of the sample production process. No systematic investigation of STM-TERS on different metals has been presented so far.

In this work, we show experimental TERS data on a wide range of different metal substrates including the known Au, Ag, Cu, and Ni, which are completed by Ti, Mo, W, Al, and stainless steel. This data are accompanied by simulations of all of the metals mentioned, as well as Pd and Cr. To complete the overview, Al_2O_3, Si, and SiO_2 as representatives for nonmetal substrates were simulated, too, to obtain information on the localization and the increase of the field strength in gap-mode TERS. A geometry entirely without tip was also simulated using finite difference time domain (FDTD).

To evaluate the intensity of the EM field in the gap between a TERS tip and a metal substrate, (tip-enhanced) Raman scattering signals can be used. The contrast factor is a measure for the increase in signal from a TERS process compared with the normal Raman scattering. In this study, the contrast factor C was calculated using Eqn (1), that is, from the ratio of the enhanced (S_{tip}) and nonenhanced (S_0) Raman signals.[30]

$$C = \frac{S_{tip}}{S_0} \qquad (1)$$

Materials and methods

Confocal Raman spectra were collected on a combined atomic force microscopy/STM instrument that incorporates a quadruple grating Raman spectrometer (Ntegra Spectra, NTMDT) and on an EMCCD camera (Newton 921 UBV, Andor Newton). The tip-enhanced Raman data were acquired in the top-illumination and top-collection gap-mode configuration, as described in detail by Stadler *et al.*[24]

In TERS experiments, the excitation laser (632.8 nm, helium–neon) was carefully focused onto the approached STM tip. Subsequently, the laser was scanned over the contact area of tip and surface, and the TERS enhancement was used to optimize the overlap of the confocal laser beam with the TERS tip. The laser power at the sample in experiments with brilliant cresyl blue (BCB) was 15 µW, with thiophenol (PhS) 100 µW used (unless specified otherwise). A collection time of 1 s per spectrum was used in imaging TERS experiments. For confocal Raman measurements, spectra from BCB were recorded but with longer integration times. For PhS, spectra from the nonenhanced area in the TERS images were used for comparison.

Tip production

Scanning tunneling microscopy tips were etched from silver wire with a diameter of 0.25 mm (99.99% purity, Aldrich). As an etchant, a mixture of 1:2 (v/v) perchloric acid (Riedel-de Haën, Seelze, Germany) : methanol was prepared. The metal wire was cut to an appropriate length and immersed into the etching solution together with a ∅ 5 cm loop out of 1 mm platinum wire as a counter electrode. A voltage of 8 V was applied between the electrodes and switched off by a custom made circuit.[23,31] The etching was terminated within 10 ms of a steep

drop in current that takes place when the apex forms and the immersed part of the wire detaches. After etching, the tips were rinsed with methanol and visually inspected using a Nikon 360× stereo microscope. This tip etching procedure yields tips that combine sufficient sharpness and high enhancement with reasonable stability for STM scanning. For each TERS experiments, freshly etched silver tips were prepared unless stated otherwise.

Metal films

Gold films were produced by coating 150 nm of gold onto silicon wafers, followed by a template stripping process similar to the one described by Hegner *et al.*[5] For silver and copper films, 150 nm of metal was deposited by physical vapor deposition onto a silicon substrate, previously cleaned in piranha acid. The following pure metal substrates were purchased (MTI KJ Group, Redmond, USA) and used as received: Al(111) (single crystal), Mo (polycrystalline), Ni (polycrystalline), stainless steel (SS301, polycrystalline), Ti (polycrystalline), and W (polycrystalline).

Sample molecules

In separate measurement series, two types of samples were investigated. In the first series, a thin film of BCB (Fluka) was deposited by spin coating 10 µL of a methanolic $5x10^{-5}$ mol/L BCB solution onto flat metal substrates: Au, Ag, Cu, Mo, Ni, stainless steel, Ti, W, and Al. Spin coating is known to produce homogeneous layers on flat substrates, but as shown in Stadler *et al.*,[24] the nanoscale distribution can be heterogeneous and differ not only between samples but also between locations within the same sample. To eliminate the influence of inhomogeneities as an error source, thiophenol (PhS, Acros Organics, Acros, Geel, Belgium) deposited directly on the TERS tip was used to probe the EM field in a second measurement series. Thiols are known to bind very strongly to metals and form self-assembled monolayers (SAM). To keep the monolayers identical between measurements on several substrates, the SAM was produced directly on the tip by dipping the freshly etched tip into a solution of 10^{-4} mol/L PhS in EtOH for 30 s and subsequent rinsing with EtOH. In this way, the same SAM could be used for experiments on both the different metals as well as on the Au reference. Potential bleaching due to decomposition of the thiol molecules was investigated under irradiation with far stronger laser light (>1 mW) and found to be negligible.

Finite difference time domain simulations

For 3D FDTD simulations, a commercial FDTD solver was employed (FDTD solutions, Lumerical Solutions, Vancouver, Canada). To correctly and efficiently simulate the near-field region, a truncated tip was positioned 1 nm above the metal substrates and excited by a focused Gaussian beam from the back. The simulated region had a size of $500 \times 500 \times 1500$ nm³ with an adaptive conformal mesh and voxel sizes ranging from approximately 20 nm³ in the outer regions down to 0.1 nm³ in the gap between tip and sample (see Fig. S1(a), Supporting Information). The simulation time was 50 fs. Detailed parameters for the tip are a 10 nm cone radius, 10° cone angle, and illumination from 1 µm distance to the tip apex with a ∼4 fs, 632.8 nm Gaussian beam pulse. The focusing of the beam pulse was simulated using a thin lens approximation with a ∅ 5 mm 0.7 NA lens and a ∅ 3 mm beam consisting of 500 plane waves

to a size of approximately 650 mm forming our excitation focus shown in Fig. S1(b) (Supporting Information). The metals for the tip and the surfaces are calculated using a dielectric constant fitted to tabulated data (CRC[32] for the surface metals and Palik[33] for the silver tip) at the simulation wavelength. A conformal mesh was used in the calculation to better account for the change of refractive index in the metal–air interfaces within voxels.

Finite element calculations with the Hades3D code

We employed the computational electrodynamics code Hades3D to analyze a detailed 3D model of the TERS setup in the time-harmonic regime. The Hades3D code[34] uses the latest discontinuous Galerkin (DG) method and solves the electric field vector wave,[35] also known as *curl-curl*, Eqn (2) in the frequency domain/time-harmonic regime.

$$\nabla \times \frac{1}{\mu} \nabla \times \overrightarrow{E} - \omega^2 \left(\varepsilon - \frac{\iota\sigma}{\omega} \right) \overrightarrow{E} = -\iota\omega \overrightarrow{J_0} \qquad (2)$$

The Hades3D code discretizes Eqn (2) on a unstructured, tetrahedral mesh in three spatial dimensions. Using tetrahedral elements allows for a flexible discretization of complicated, curved geometry avoiding the staircasing effect. In addition, using tetrahedral elements allows for level of detail modeling where geometrically delicate but physically immensely relevant geometry needs to be discretized with small elements, and larger elements are used elsewhere. When working in the time-harmonic regime, measured complex refractive index data[32] can be used directly. For the simulation of the TERS setup, identical geometry parameters were used for the tip. The simulation setup consisted of the 3D tip that hovered over a hexahedral substrate block with a square cross section. Here, in stark contrast to the FDTD analysis, the TERS setup was modeled with optimal efficiency. In particular, the TERS setup was fitted into an oval-shaped computational domain, not wasting tetrahedral elements. Even today, given seemingly unlimited compute power, it is essential to model nano-optical setups with the highest possible efficiency, because the solution of the complex linear systems that results from the DG discretization is a challenging task. Our model counted 4 million degrees of freedom; that is, the linear system was a square matrix with 4 million rows and columns. A representation of the EM problem setup is shown in Fig. 1. The size of tetrahedral elements used for the discretization of the TERS setup comprised several orders of magnitudes, from a fraction of a nanometer, close to the tip, up to several tens of nanometers further away from the tip. The mesh was created with the open source GMSH[36] mesh generation program. The computational domain was transparently truncated with a first-order absorbing boundary condition.[35,37] It is one of the strengths of the first-order absorbing boundary condition to truncate almost any convex geometry in a computational domain; in our case, it was an oval-shaped boundary. Although the perfectly matched layer might reduce spurious reflections even further, its practical application is usually restricted to hexahedral shapes; thus, there is a tendency of wasting unnecessary tetrahedral elements. The EM problem is excited through an incoming transverse-electric-magnetic wave at a wavelength $\lambda = 632.8$ nm.
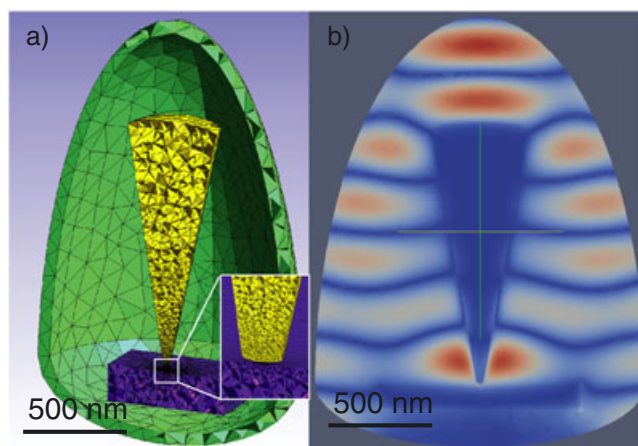

Figure 1. (a) Computational domain of the Hades3D finite element calculations with a refined grid towards the tip apex. The green shell shows the outer transparent boundary, minimizing reflections with an optimized shape to reduce computational cost. (b) $|E^2|$ intensity of electromagnetic field upon illumination with a 632.8 nm laser from the top.

Results and discussion

Experimental determination of the electromagnetic field

To experimentally investigate the EM field in the TERS gap, resonant BCB molecules were used to probe the field intensity. On all surfaces, a thin layer of dye molecules was homogeneously distributed by spin coating. With an approached tip, the laser was then scanned over the contact area. The tip then probes the scanned laser focus, resulting in TERS enhancement when both overlap. At every pixel, a Raman spectrum was collected resulting in an enhancement map of an area at and around the tip. The signal collected on the CCD camera is mainly influenced by three factors: the number of molecules contributing to the signal, the enhancement of the tip in use, and the influence of the metal substrate on the field in the gap. The distribution of molecules on the surface of the substrate was expected to be homogeneous. To compensate for differences between different metal substrates, confocal reference spectra were collected. To evaluate the Raman intensity in the spectra, the luminescence background of the spectra was subtracted to yield pure Raman contributions. The contrast factor between two Raman bands (confocal + TERS signal) was calculated according to Eqn (1) to eliminate the influence of the density of molecules on the surface. The contrast factors calculated from two different tip enhancement maps (metal/Au) were then divided to cancel the influence of the specific enhancement of the tip in use. The relative intensity of a specific metal compared with Au should now be neither sensitive to the tip used nor be influenced by the number of molecules on the surface and thus represent the pure contribution of the metal surface to EM field strength in the TERS gap.

In Fig. 2, two single spectra from within the TERS hot spot of the same tip on Cu and Au surfaces are shown, as well as the corresponding confocal Raman spectra (from the same area, collected with tip retracted after refocusing on the surface). From these four spectra, both contrast factors for Au and Cu can be calculated as shown in Eqn (3). Thus, with these four spectra, the contrast of the tip on Cu was 21% of the contrast of the same tip on Au (i.e., the contrast was smaller by a factor of 5). For obtaining the values in Table 1, the same
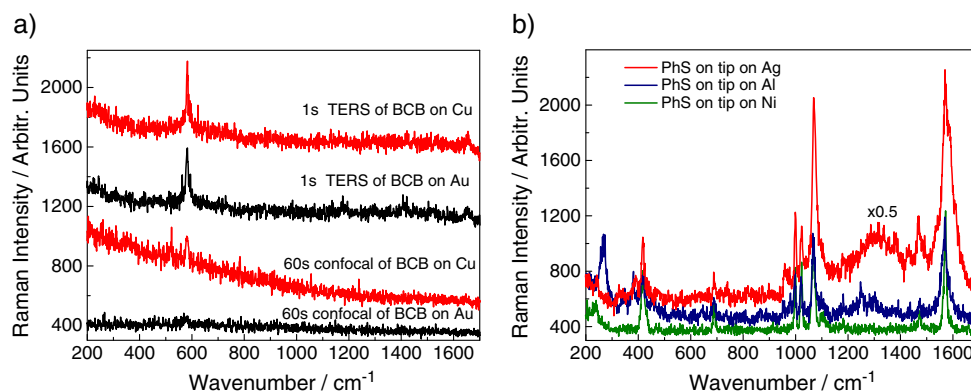
Figure 2. (a) 1 s tip-enhanced Raman spectroscopy (TERS) spectra from brilliant cresyl blue (BCB) on Au (red) and Cu (red), with the corresponding 60 s confocal Raman spectra, all recorded using the same tip. Spectra are offset for clarity, and three spikes were removed from the confocal spectrum on Cu. (b) Point TERS spectra from PhS on the tip in contact with different metal substrates: Tip on Ag (red), Ni (green), and Al (blue), all showing clear signatures of PhS from the self-assembled monolayers on the tip. Intensities differ due to different enhancements of the tips in use for the respective experiment.

Table 1. Comparison of the electromagnetic field enhancement in the gap between various metals and a silver tip, using two different simulation techniques and two different experimental approaches. All theoretical values have been normalized to the value of a tip on Au. Experimental values were normalized to the intensity measured on a Au substrate using the same tip

Metal	E^2 (FDTD)	E^4 (FDTD)	E^2 (FE)	TERS (BCB)	TERS (PhS)
Au	1	1	1	1	1
Cu	0.92	0.848	–	0.16 ± 0.11	–
Ag	0.81	0.654	0.559	0.23 ± 0.05	0.77
Al	0.63	0.402	–	–	–
Pd	0.61	0.375	–	–	–
Pt	0.55	0.297	–	–	–
Ni	0.53	0.281	–	0.07 ± 0.06	0.72
Cr	0.51	0.264	–	–	–
Ti	0.45	0.199	–	$0.12 + 0.14 - 0.12$	–
Mo	0.44	0.194	–	$0.11 + 0.16 - 0.11$	–
W	0.41	0.166	–	–	–
Al_2O_3	0.09	–	–	–	–
SiO_2	0.05	0.003	–	–	–
Tip only	0.05	0.003	–	–	–

FDTD, finite difference time domain; FE, finite element; TERS, tip-enhanced Raman spectroscopy; BCB, brilliant cresyl blue.

approach, with several TERS spectra from the TERS hot spot and background spectra from confocal images, was used.

$$\text{Exemplary Calculation}: \left. \begin{array}{l} C_{Cu} = \dfrac{S_{nearfield,Cu}}{S_{farfield,Cu}} = \dfrac{410\frac{cts}{s}}{\frac{160cts}{60s}} = 154 \\[12pt] C_{Au} = \dfrac{S_{nearfield,Au}}{S_{farfield,Au}} = \dfrac{370\frac{cts}{s}}{\frac{30cts}{60s}} = 740 \end{array} \right\} \dfrac{C_{Cu}}{C_{Au}}$$
$$= \frac{154}{740} = 20.8\%$$

(3)

Analogous evaluations were carried out for Ag, Cu, Ni, Ti, and Mo with several tips each, resulting in the Raman(BCB) values in Table 1 and the blue triangles in Fig. S2. Repetitions of these experiments showed only little reproducibility, as indicated by the large error bars. The cause for this is most likely nanoscale concentration differences on the metal surfaces. This behavior

has already been observed in other samples, even if they appear homogeneous in confocal Raman measurements.[24]

To eliminate effects due to nanoscale concentration differences when probing the molecules, a SAM of PhS was deposited on the etched silver tips. The same tip and thus the identical monolayer were then used in consecutive experiments to again probe the EM field in the TERS gap on Au and other metals. Potential bleaching was found to be negligible, even upon irradiation of the tip with >1 over 1. Results from PhS on a Ag tip approached to Ag and Ni are presented in Table 1, showing far better agreement with the results from simulations. The data points represent the intensity on Ag and Ni respectively each divided by the intensity of the same tip on Au. The measurements on Ni and Ag show signal intensities of 72% and 77% compared with that on Au with the same tip, and thus clearly indicate the suitability of these substrates for TERS (a visual representation for the different metals is given in Fig. S2 (Supporting Information)). A drawback of using a thiol monolayer as a probe for the EM field is the overall low signal intensity. In many experiments on metal surfaces, specific bands

of PhS were detected but could not be adequately quantified because of the high noise level. Although an experimental quantification was not possible in all cases, a similar behavior in TERS with small losses within one order of magnitude for all metal surfaces can be expected. This is also supported by simulations. For nonmetal substrates, far higher losses are to be expected, making conductive Si surfaces or ITO glasses a poor choice for gap-mode TERS experiments. Experiments on nonmetal substrates (ITO) support this estimate (data not shown). The gap-mode effect (comparison of a tip in free space without surface and a tip on Au) delivers an additional enhancement of 20–40 in the EM field intensity $|E|^2$, with even stronger impact on the Raman intensities, which increase by a factor of 50 to >300.

The comparison of the two different sets of TERS experiments on BCB and PhS shows major differences on the same metal substrates. Potential sources for these differences are not only potential bleaching of the BCB dye and nanoscale differences in the distribution of BCB but also the location of the PhS molecules on the tip rather than on the surface. Although only a nanometer wide, gradients in the EM field between tip and surface could account for part of the differences in between experiments.

Computational calculation of the electromagnetic field

The FDTD method has been developed over the last decade and now reached considerable maturity. Over the course of the years, a wide span of applications has been analyzed successfully with the FDTD approach: from nearly static problems up to the optical region of the EM spectrum. On the other hand, there is increasing evidence[38] that the FDTD method is not up to the task of reliably modeling nano-optical problems. Even worse, the publication[38] concludes that the FDTD method would not converge to the true solution because of the staircasing approximation, when discretizing curved geometry, even when the voxels in the Cartesian sampling grid become negligibly small. Thus, FDTD increasingly becomes a side-track method for nano-optics because it struggles with the wide span of characteristic length scales typically encountered there. In marked difference to microwave EM problems where the size of the elements usually amounts to $\lambda/10$ or $\lambda/20$, in nano-optics, the size of elements easily tends to $\lambda/1000$ or even smaller. Additionally, the radius of curvature for geometry encountered in nano-optics is on the order of a few nanometers only. Consequentially, the discretization of geometry needs to adapt. This is where the DG variant[39] of the finite element (FE) method has its advantages; given good mesh generation software, it is a manageable task to create a mesh with level of detail, whose element sizes varies over several orders of magnitude. Thus, a good approximation of curved geometry becomes available. Solving the resulting discretized system, that is, a large, sparse complex symmetric matrix, is a formidable task,[39] which in itself is an active research topic. However, there is a silver line over the horizon[40] that will soon allow to solve ultra-large linear systems, with several tens of millions of degrees of freedom, efficiently; this will eventually enable the accurate and reliable analysis of realistic structures with confidence. In conclusion, we maintain that the FE method is the method of choice, when analyzing complicated geometry and material systems is of the essence.

A first set of calculations was designed to reproduce the known field distribution in TERS to ensure credibility of the FDTD results. Therefore, 3D FDTD field distributions from similar systems calculated in the literature[14] were recalculated using our model. Very similar results were found, as shown in Fig. S3 (Supporting Information). In a second step, the influence of the gap distance in our system was systematically varied with a surface approaching the tip from infinite distance down to 0.25 nm. An animation of $|E|^2$ in the x,z plane from the simulation with decreasing distance is given in Fig. S4 (Supporting Information). The behavior of the EM field in the movie compares well to known distance dependence in TERS.[14–16] It clearly shows increased fields around the tip apex already without the surface as well as a further localization and increase of the field upon approach of the metal surface. The reason for better confinement and the rising magnitude of $|E^2|$ is the induction of a mirror dipole in the metal surface by the dipole in the tip apex. A potential explanation for the increased fields could be efficient coupling of the surface plasmons of tip and surface.

Figure 3(a) displays view of a Ag tip in tunneling distance (1 nm) to a gold surface with a logarithmic scale. Surface plasmons with increasing intensity can be seen on the side of the tip approaching the apex. In the animation in Fig. S5 (Supporting Information), the phase of the calculated FE solution is varied from $-180°$ to $180°$ to illustrate the movement of the plasmons along the side of the tip towards the apex, creating a very strong and localized EM field in the gap. In the linear intensity view in Fig. 3(b), the very strong localization of the field leading to increased resolution in TERS is visualized.

The influence of the metal substrate was determined from the maximum intensity of the E^2 field in the FDTD and FE calculations. The calculated values are plotted in Fig. S2. The numerical values in Table 1 show that the loss of EM field intensity, when replacing the most strongly enhancing and most frequently used Au surface by a different metal, is in the region of a factor of only 1.5 to 3 for metals but considerably higher for nonmetals. A visual comparison of the EM field distribution in the gap for different metals calculated by FDTD is shown in Fig. S6 (Supporting Information). Both calculation methods and practical experience support this, although minor differences between the calculation methods do remain. When compared with an experimental Raman intensity, the EM field intensity $|E|^2$ cannot be used directly but has to be squared, as the measured Raman intensity scales with $|E|^2_{\lambda\text{Laser}} \cdot |E|^2_{\lambda\text{Raman}}$. Although the wavenumber of the
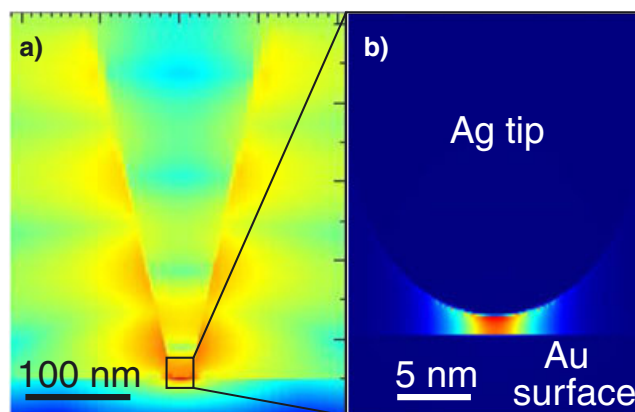

Figure 3. $|E^2|$ field distribution of a Ag tip approached to a Au surface using finite difference time domain: (a) log view over the entire tip length visualizes plasmons on the flanks of the tip increasing in intensity towards the tip apex; (b) linear color scale view of the tip apex area shows localization of the field to a few nanometers.

Raman scattered light changes within the same experiment for different bands, it is still reasonably close to the laser wavelength; as an approximation, both can be considered equal, and the enhancement can be calculated as $|E|^4$. The approximation can be one explanation for some remaining differences between experiment and calculations. The more correct approach using the effective Raman wavelength cannot be incorporated in the calculations at present.

Conclusions

Results from both experiments and calculations were used to investigate the suitability of different metal and nonmetal surfaces for use in TERS. With a thin dye film used, enhancement could be shown on all experimentally investigated metal substrates but not yet on nonmetal substrates. The experimental quantification of the EM field turned out to be difficult because of low signal intensity or inhomogeneous distribution of molecules on the nanometers scale. Yet, the experimental proof for the presence of the enhancement can be combined with the numerical values from two independent sets of simulations. Both simulations suggest TERS intensities on metal substrates to be within one order of magnitude of those of Au. This clearly shows that not only Au but also a number of other metal substrates is well suited for TERS experiments and can be used when gold has unwanted specific interactions with the sample (especially when Au–S interactions are undesired), when it is difficult to transfer a sample onto the gold substrate or simply because it is too expensive. The drawbacks of changing the substrate are in most cases a slightly reduced conductivity resulting in a less reliable feedback during STM scanning and occasionally rougher surface topography.

Other simple theoretical calculations of the effect of the substrate on the EM enhancement using a dipole model were conducted by Zhang et al.[19] (Fig. 6a). They map the enhancement underneath a TERS tip depending on Re(ε) and Im(ε), showing that the real part of ε determines the best wavelength for resonance and Re(ε) should be close to -2. The numerical value of -2 is only correct for a spherical tip, which leaves the exact shape as a parameter to tune the TERS performance in a certain wavelength and metal combination. The imaginary part of the refractive index determines the extent of the enhancement that can be reached with an optimum approaching zero. The calculated and measured enhancement for the metals used in this work fit to the expected enhancement based on the ε values.

Potentially, two additional parameters could improve the TERS enhancement using metal substrates: on the one hand, using a suitable laser wavelength, the losses from Im(ε) in any dispersive metal can be reduced. At the same time, if wavelength can be optimized to efficiently excite the resonance frequency of the coupled tip-sample system, any sample can be measured more efficiently. Determination of the coupled influence of both these effects using a tunable laser source in the visible range could prove this. Such measurements could furthermore be combined with 3D simulations to quantify the contributions of both effects to the total field enhancement.

Envisioning a more general use of TERS, a wide range of affordable substrates is necessary to allow more widespread application of the technique. If a very cheap, flat, for example, stainless steel sample support could be used for most experiments where the intensity gain from gap-mode TERS does not have to be optimal, consumable costs for TERS would be greatly reduced. Samples present on any working metal substrate, for example, for monitoring the production of CVD graphene on Cu, could be investigated directly by TERS during production without further processing. This could bring TERS one step further towards an established standard for everyday routine analytics.

Supporting information

Supporting information may be found in the online version of this article.

References

[1] R. M. Stockle, Y. D. Suh, V. Deckert, R. Zenobi, *Chem. Phys. Lett.* **2000**, *318*, 131.
[2] M. S. Anderson, *Appl. Phys. Lett.* **2000**, *76*, 3130.
[3] N. Hayazawa, Y. Inouye, Z. Sekkat, S. Kawata, *Opt. Commun.* **2000**, *183*, 333.
[4] B. Pettinger, G. Picardi, R. Schuster, G. Ertl, *Electrochemistry* **2000**, *68*, 942.
[5] M. Hegner, P. Wagner, G. Semenza, *Surf. Sci.* **1993**, *291*, 39.
[6] K. Dickmann, F. Demming, J. Jersch, *Rev. Sci. Instrum.* **1996**, *67*, 845.
[7] M. Iwami, Y. Uehara, S. Ushioda, *Rev. Sci. Instrum.* **1998**, *69*, 4010.
[8] W. H. Zhang, B. S. Yeo, T. Schmid, R. Zenobi, *J. Phys. Chem. C* **2007**, *111*, 1733.
[9] B. Ren, G. Picardi, B. Pettinger, *Rev. Sci. Instrum.* **2004**, *75*, 837.
[10] C. Williams, D. Roy, *J. Vac. Sci. Technol. B* **2008**, *26*, 1761.
[11] V. Snitka, R. D. Rodrigues, V. Lendraitis, *Microelectron. Eng.* **2011**, *88*, 2759.
[12] X. D. Cui, D. Erni, W. H. Zhang, R. Zenobi, *Chem. Phys. Lett.* **2008**, *453*, 262.
[13] R. Esteban, R. Vogelgesang, K. Kern, *Phys. Rev. B* **2007**, *75*, 195410.
[14] R. M. Roth, N. C. Panoiu, M. M. Adams, R. M. Osgood, C. C. Neacsu, M. B. Raschke, *Opt. Express* **2006**, *14*, 2921.
[15] B. Pettinger, K. F. Domke, D. Zhang, G. Picardi, R. Schuster, *Surf. Sci.* **2009**, *603*, 1335.
[16] Z. Yang, J. Aizpurua, H. Xu, *J. Raman Spectrosc.* **2009**, *40*, 1343.
[17] P. Drude, *Ann. Phys.* **1900**, *306*, 566.
[18] P. Drude, *Ann. Phys.* **1900**, *308*, 369.
[19] W. H. Zhang, X. D. Cui, O. J. F. Martin, *J. Raman Spectrosc.* **2009**, *40*, 1338.
[20] D. Zhang, K. F. Domke, B. Pettinger, *Chemphyschem* **2010**, *11*, 1662.
[21] G. Picardi, M. Chaigneau, R. Ossikovski, C. Licitra, G. Delapierre, *J. Raman Spectrosc.* **2009**, *40*, 1407.
[22] K. F. Domke, D. Zhang, B. Pettinger, *J. Am. Chem. Soc.* **2006**, *128*, 14721.
[23] W. H. Zhang, X. D. Cui, B. S. Yeo, T. Schmid, C. Hafner, R. Zenobi, *Nano Lett.* **2007**, *7*, 1401.
[24] J. Stadler, T. Schmid, R. Zenobi, *Nano Lett.* **2010**, *10*, 4514.
[25] J. Steidtner, B. Pettinger, *Phys. Rev. Lett.* **2008**, *100*, 236101.
[26] T. Deckert-Gaudig, V. Deckert, *J. Raman Spectrosc.* **2009**, *40*, 1446.
[27] Y. Hirata, K. Sakamoto, Y. Uehara, S. Ushioda, *Jpn. J. Appl. Phys.* **2009**, *48*, 110206.
[28] B. Ren, G. Picardi, B. Pettinger, R. Schuster, G. Ertl, *Angew. Chem. Int. Ed.* **2005**, *44*, 139.
[29] J. Stadler, T. Schmid, R. Zenobi, *ACS Nano* **2011**, *5*, 8442.
[30] B.-S. Yeo, T. Schmid, W. Zhang, R. Zenobi, in *Infrared and Raman Spectroscopic Imaging*, Wiley, New York, **2009**, pp. 473–499.
[31] J. P. Ibe, J. P. P. Bey, S. L. Brandow, R. A. Brizzolara, N. A. Burnham, D. P. DiLella, K. P. Lee, C. R. K. Marrian, R. J. Colton, *J. Vac. Sci. Technol., A* **1990**, *8*, 3570.
[32] W. M. Haynes, *Crc Handbook of Chemistry and Physics, Ed. 92 (2011–2012)*, CRC Press, Boca Raton, **2011**.
[33] E. D. Palik, G. Ghosh, *Handbook of Optical Constants of Solids Five-Volume Set*, Academic Press, San Diego, **1991**.

[34] B. Oswald, *Opt. Express* **2012**, *work in progress*.

[35] J. L. Volakis, A. Chatterjee, L. C. Kempel, *Finite Element Method for Electromagnetics Antennas, Microwave Circuits, and Scattering Applications*, IEEE Press, New York, **1998**.

[36] C. Geuzaine, J. F. Remacle, *Int. J. Numer. Methods Engineering* **2009**, *79*, 1309.

[37] J. Jin, *The Finite Element Method in Electromagnetics* (2nd edition), Wiley, New York, **2002**.

[38] F. Kaminski, V. Sandoghdar, M. Agio, *J. Comput. Theor. Nanosci.* **2007**, *4*, 635.

[39] D. Sarmany, F. Izsak, J. J. W. van der Vegt, *J. Sci. Comput.* **2010**, *44*, 219.

[40] B. Engquist, L. X. Ying, *Multiscale Model. Sim.* **2011**, *9*, 686.

[41] B. Oswald, P. Leidenberger, *J. Comput. Theor. Nanosci.* **2009**, *6*, 784.

[42] B. Oswald, A. Fomins, A. Fallahi, P. Leidenberger, P. Bastian, *J. Comput. Theor. Nanosci.* **2011**, *8*, 1573.